Molecular Dynamics of a Polymer in Mixed Solvent: Atactic Polystyrene in a Mixture of Cyclohexane and *N,N*-Dimethylformamide

Qi Sun and Roland Faller*

Department of Chemical Engineering & Material Science, University of California at Davis, One Shields Avenue, Davis, California 95616

Received: October 8, 2004; In Final Form: May 14, 2005

Local structural and dynamic properties of atactic polystyrene in a mixed solvent of cyclohexane (CH) and *N,N*-dimethylformamide (DMF) have been investigated using molecular dynamics simulations. We measure local conformations in the polymer and classify them by distance and angle distribution histograms. End-to-end distances and structure factors are employed to describe the static structure of polystyrene chains. Polystyrene concentration, including 1.6%, 4.8%, and 14% (by weight), and solution temperatures of 300, 330, or 360 K are used to elucidate the concentration and temperature dependencies of the solvation by the two solvents. Both solvent molecules preferentially approach the phenyl rings. At lower temperatures, polystyrene dissolves more favorably in cyclohexane. With rising temperature DMF molecules approach more closely with the oxygen oriented toward the phenyl rings. Additionally, the global and segmental relaxation times of the chains decrease and the system becomes more homogeneous. The segmental and global dynamics of polystyrene show different concentration behaviors: the reorientation times of solvent molecules and segments of polystyrene increase with concentration while the global dynamics of polystyrene decelerates as the concentration is changed from 1.6% to 4.8% but accelerates when the concentration rises to 14%. We conclude that the change of concentration from 4.8% to 14% qualitatively marks the change from a dilute to a semidilute solution. The diffusion constants of the small molecules and corresponding activation energies have also been measured. Our simulation data are compared with available experimental results and we find a satisfactory agreement.
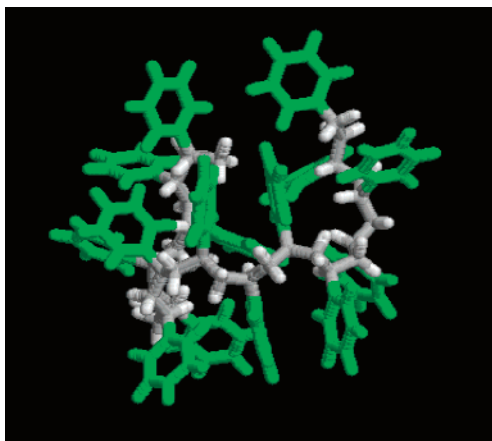
1. Introduction

Polymers are an interesting field of study due to their various applications. Polymer solutions are of great interest from both a fundamental viewpoint and due to their various technical applications.[1] Solvents significantly alter polymer properties and can lead to favorable or unfavorable changes. Elucidating the solvation mechanisms will help understand the basic behavior of polymer chains in mixed solvents and by this help characterize polymeric systems at industrially important state points. Polymers in pure solvent have been simulated by several researchers,[2−5] but there are only a few studies on how the polymer chains influence the solvent dynamics.[6,7] To the best of our knowledge this is the first study of a polymer−mixed solvent system studied in atomistic detail. Polystyrene as an inexpensive and hard plastic is widely used in automobiles, construction, and packaging industries. Most polymerization processes lead to the atactic conformation. Atactic polystyrene (PS) has been investigated by both experiments[8−11] and computer simulations.[11−16] This study focuses on the liquid structure and dynamics of small solvent molecules in the neighborhood of atactic PS oligomers in dilute or semidilute solution. Experimental studies of systems with more than one type of solvent exist,[17−19] and we will compare to available data. Our system contains one type of polymer in two solvents with different properties. The physical properties of a polymer solution depend on solvent properties, temperature, and concentration. We focus on atomistic simulations of PS dissolved

in a mixture of cyclohexane (CH) and *N,N*-dimethylformamide (DMF). Cyclohexane is a rather spherical organic molecule and is experimentally known to be a good solvent for polystyrene.[20,21] DMF is one of the simplest amide compounds and has interesting properties. It has a large dipole moment and is a poor solvent for PS at room temperature.[22] Since in good solvents the polymer segments tend to be surrounded by solvent particles rather than other segments, the net interaction between polymer segments in good solvents is repulsive and the excluded volume parameter is large. On the other hand, the excluded volume parameter of poor solvents can be small or even negative, depending on temperature. It is interesting how the polymer characteristics depend on the type of solvent that is in the system.

Atactic PS is more abundant than the isotactic or syndiotactic conformation. Head-to-tail polymerization dominates in the case of atactic PS. Models containing only head-to-tail units with random chiralities at the asymmetric carbons are investigated throughout this article. The dyads tie to the tacticity of PS. The addition of a monomer is called "meso" if the functional group adds on the same side as that of the previous monomer, or otherwise "racemic". The chiralities of the PS chains are controlled by the ratios of meso to racemic in every single chain. Figure 4 can be viewed as an example. The equilibrium conformation of a single chain of PS of length 15 monomers at atmospheric pressure and a temperature of 300 K is shown in Figure 1. A systematic and comparative investigation of this polymer and solvent mixture will help us to obtain a more thorough understanding of the solvation mechanism. These

---

* To whom correspondence should be addressed. E-mail: rfaller@ucdavis.edu.

Molecular Dynamics of a Polymer in Mixed Solvent

J. Phys. Chem. B, Vol. 109, No. 33, 2005 **15715**

Figure 1. Snapshot of the atactic PS conformation ($T = 330$ K, $P = 100$ kPa) of the single PS chain with 15 monomers.

TABLE 1: Equilibrium Angles and Bond Length Parameters for DMF

angle	ϕ_0 (deg)	k (kJ/(mol rad^2))	bond	l_b (nm)
H−C−O	127.6	334.944	C=O	0.1229
H−C−N	109.5	293.076	C−N	0.1335
O−C−N	122.9	334.944	C_{sp^3}−N	0.1449
C−N−C_{sp^3}	121.9	209.34	C_{sp^3}−H	0.109
C_{sp^3}−N−C_{sp^3}	116.2	209.34	C−H	0.109
H_{sp^3}−C_{sp^3}−N	109.5	146.538		
H_{sp^3}−C_{sp^3}−H_{sp^3}	109.5	146.538		

TABLE 2: Force Field Parameters of the Nonbonded Interactions for DMF^a

atom	M (amu)	ϵ (kJ/mol)	σ (nm)	q
C	12	0.3601	0.3816	0.54
N	14	0.7118	0.3648	−0.43
O	15.9949	0.6502	0.3166	−0.51
C_{sp^3}	12	0.336	0.35	0.21
H_{sp^3}	1.007825	0.21	0.257	0
H	1.007825	0	0	−0.02

^{a} M is the atom mass, ϵ is the interaction strength, σ is the interaction radius, and q is the charge of the atom.

studies include local structure, dynamic properties, and thermodynamic measurements. Detailed microscopic structure and dynamic properties are investigated through molecular dynamics. The GROMACS[23] simulation package was used in fully atomistic simulations to investigate the behavior of the polymer and solvent mixture system on the local scale.

2. Details of the System

Systems containing one, three, or ten 15-monomer chains of atactic polystyrene were simulated in a mixed solvent of 500 molecules of *N,N*-dimethylformamide (C_3H_7NO) and 674 molecules of cyclohexane (C_6H_{12}). Chalaris et al.[24] compared several force field models for *N,N*-dimethylformamide and concluded that the six-interaction-site OPLS can describe not only the thermodynamic and structural properties, but also the transport properties of the system with good accuracy in a wide temperature range at ambient pressure. Therefore we have chosen the OPLS computational model for liquid DMF. The detailed bond, angles, and nonbonded interaction parameters are listed in Tables 1 and 2.

For the force field of polystyrene, we use the Lennard-Jones parameters of Jorgensen and Severance.[25] This all-atom model has small partial charges on the carbon and hydrogen atoms of phenyl groups. The model reproduced the electric quadrupole moment of the benzene molecules and was confirmed by Müller-

TABLE 3: Details of the Simulated Systems^a

				ρ/ρ_{exp} (kg m^{-3})		
N_P	N_{CH}	N_{DMF}	t_{sim} (ns)	300 K	330 K	360 K
1	1	674	500	10	861.8/857	829.51/856	794.45
2	3	674	500	10	869.2	835.98	810.22
3	10	674	500	10	886.4	855.21	824.65

^{a} N_P is the number of atactic PS chains, N_C is the number of cyclohexane molecules, and N_{DMF} is the number of DMF molecules. t_{sim} is the simulated time for the systems. Additionally, the densities ρ are shown for the temperatures considered.

Plathe.[6] In total, the following contributions to the interaction potential were considered: (1) bending potential for all the angles (bonds are constrained using the LINCS method),[26] (2) torsion potential for all the backbone and phenyl ring carbons, and (3) improper, i.e., harmonic, torsion potentials, which are used to achieve the desired geometry in the force field and are defined as:

$$K_t[t_{ijkl} - t_0]^2$$

where t_{ijkl} is the torsion angle spanned by the atoms i, j, k, and l, t_0 is the equilibrium torsion angle, and K_t is the force constant (the latter was used for three purposes: first, all the carbons of phenyl groups have to be coplanar; second, the hydrogen atoms of the phenyl groups have to be in the same plane as carbons of phenyl groups; and third, the hydrogen atoms bonding to the backbone carbons maintain the improper torsion angle at 180°); and (4) nonbonded Lennard-Jones interactions between all atoms four or more bonds away. No internal nonbonded interactions in CH are considered and the nonbonded interactions between all atoms of any phenyl group in PS are excluded. We used the cyclohexane force field described in detail in ref 27 with the torsions defined in ref 7.

The atactic configuration of PS is generated by head−tail connection with the aromatic groups located at either side of backbone carbon randomly. Correspondingly, each chain has a different arrangement. The overall ratio of meso to racemic at various concentrations is 1:1. An overview of all the systems and the resulting densities in the simulations are shown in Table 3. The densities are compared against available experimental data from Park.[28] Atomistic simulations were performed using molecular dynamics at temperatures of 300, 330, or 360 K and a pressure of 101.3 kPa with a time step of $\delta t^* = 0.002$ ps. The simulation box had an average size around 5.6−6.0 nm in all directions. A truncated and shifted Lennard-Jones potential for the excluded-volume interaction with a cutoff of 0.9 nm between all atoms was used. Constant temperature and pressure were ensured by using the Berendsen weak coupling method[29] with coupling constants of 0.2 ps for temperature and 1 ps for pressure, respectively. The pressure coupling used an anisotropic pressure control with a compressibility of 1.12×10^{-6} bar^{-1} for the three Cartesian directions independently.

3. Equilibration

In atomistic simulations, the way a system is initially set up and equilibrated is crucial. Thus, we describe the equilibration procedure for our systems in detail. The ten chain system with 674 CH and 500 DMF is taken as an example. The configuration of one PS chain in a vacuum was set up first. Chains are different due to the atactic nature of the polymer. An energy minimization process using steepest descent can be used to generate a different atactic conformation from any chain if the force field is switched; in a vacuum the phenyl rings can easily

switch with the hydrogens. This procedure was used to generate ten chains of 15-mer PS in total from one parent chain. Various ratios of meso to racemic structures are employed to obtain an atactic structure with random chiralities. Meso or racemic structure can be characterized by the angle between the normal vector of the three backbone carbons and the vector connecting the backbone carbon and the phenyl group carbon and verified during simulation. Steep descent is very fast in the early stage of energy minimization. Conjugate gradient becomes more efficient closer to the energy minimum. It is most efficient when a steepest descent step is performed every once in a while together with the conjugate gradient method than when using either one exclusively. However, conjugate gradient cannot be used with constraints, so the constraints had to be changed to harmonic bonds for these minimizations. After this initialization, we combine all ten PS chains with a CH and DMF mixture. At the primary stage, atom overlaps were inevitable. A subsequent energy minimization can remove the closest contacts between particles. However, it may lead to phenyl groups and small solvents, especially CH with a cyclic structure, crossing and then connecting which ultimately generates a system with an unrealistic topology. Special attention should be taken by visualizing the system carefully right after the energy minimization process.

The equilibration procedure continues with a microcanonical simulation with a short time step of 0.1 fs. The box was obtained by connecting eleven small boxes. One contained 674 CH molecules and 500 DMF molecules and the rest contained one PS chain each. The simulation started at an initial density of around 76.0 kg/m^3, at this low density the segmental motion of the polymer is extremely fast and equilibration of the internal degrees of freedom readily achieved. The time step was gradually increased from 0.1 to 2 fs. After the system had become stable under microcanonical conditions, the Berendsen thermostat and barostat were switched on with a temperature coupling constant of 0.2 ps and a pressure coupling constant set of 0.1 ps to compress the system to the correct density. The velocities of the particles were reset from a Maxwell−Boltzmann distribution corresponding to 300 K before each run. Additionally, regular compression with a linear compression factor of 0.9 in each direction combined with minimization was performed. The compression factor was selected to smooth the compression and avoid severe changes to the system at once, which again would lead to topological problems. As the system approached the correct density, the pressure coupling had a greater effect on the system and the interaction potential energy was more effective in compressing the molecules. After a density of 600 kg/m^3 was reached, only the pressure coupling was applied and the system quickly attained equilibrium density.

After equilibration, the production runs were started. The relaxation time of the end−end vector of the polymer is the largest characteristic time of the system. It was evaluated to test if the polymer loses its initial structure memory. The production runs typically took 10 ns, which is slightly shorter than the longest relaxation time at the lowest temperature. Shorter run times were sufficient at higher temperatures.

4. Local and Global Structure of the System

An atactic 15-monomer chain is formed through random connections between monomers. The configurations of the consecutive benzene rings can explain details of the local solvent structure. The local configuration of the side rings of PS can be characterized by the distribution of the distances and angles of the centers of mass of the side rings. All histograms are
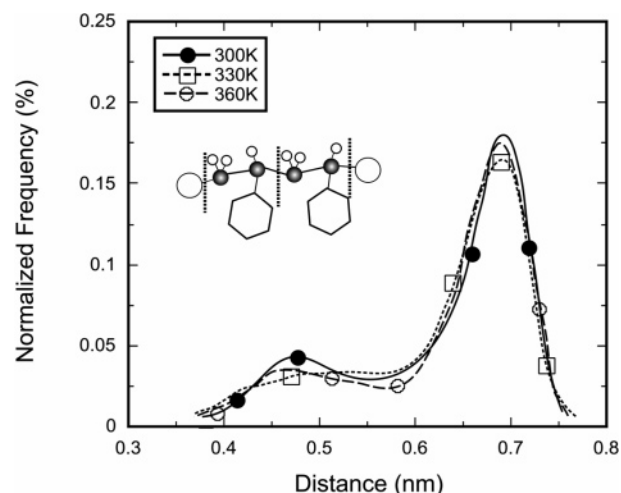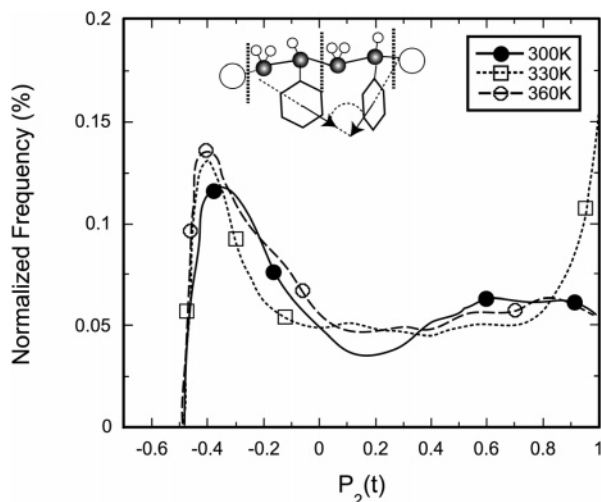

Figure 2. The normalized frequency: distances between the consecutive side rings obtained from the simulation at 300, 330, and 360 K.

normalized. The distance histograms between consecutive benzene rings are shown at 300, 330, and 360 K in Figure 2. The distances between the centers of neighboring rings range from 0.35 to 0.75 nm. The distance can be as short as 0.35 nm in the case of a compact meso structure and it can be as long as 0.75 nm as the bulky phenyl rings are located at the opposite side of the backbone. We observe two peaks for each temperature. The first is not so noticeable when temperature increases and over all the area under the two peaks remains constant. The first peak in the histograms is the result of two consecutive rings at the same side of the backbone. Since the distance between the two backbone carbons is 2 × 0.2545 = 0.590 nm in the case of the fully stretch status, it is expected the distance range is from 0.35 to 0.55 nm while phenyl rings are located at the same side of the backbone. Increasing temperature facilitates the torsion movement around the backbones, which drives the phenyl rings to more evenly distribute around the first peak region. The second peak is the result of two subsequent phenyl rings taking on a different torsional angle such as 120° or −120° if the neighbor is at 0°. Torsional angle means the dihedral around the chain backbone, which makes the phenyl rings favor three positions in space. Overall the second peaks at various temperatures are the same since the underlying structures are strongly fixed. The difference in height of the two peaks shows that the larger distance is more favorable and a few of the meso dyads are there as well. To characterize this local structure in more detail we investigate the angles between consecutive side rings as shown in Figure 3. The angle between normal vectors of the ring plane is used to determine the angle orientation of the side rings. As neither the chain nor the rings have directionality and thus the sign of the scalar product is meaningless, the second Legendre polynomial $P_2(t)$ is more appropriate and it is defined as
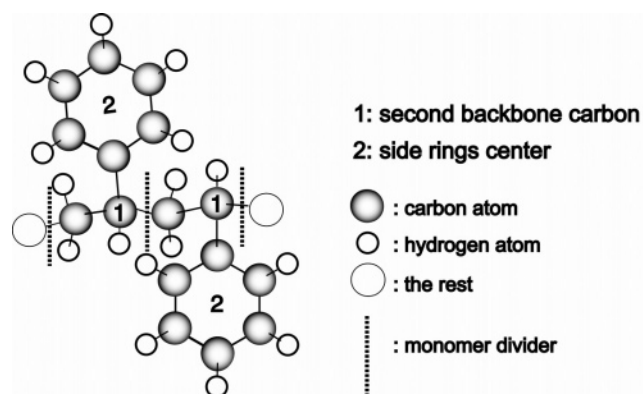
$$P_2(t) = \frac{1}{2}\langle 3(\bar{u}_i \cdot \bar{u}_j)^2 - 1 \rangle$$

$\bar{u}_i$ and $\bar{u}_j$ are the normal vectors of the rings. The scalar product $\bar{u}_i \cdot \bar{u}_j$ corresponds to the cosine of angles between the two vectors. $P_2(t)$ carries information indicating the preference of specific angles. There is a noticeable peak around −0.5 (≈90°) for the angle distribution at all three temperatures. This peak is consistent with quadrupolar interaction between the phenyl groups.[6] There are two peaks at 330 K, one corresponds to a perpendicular constellation and the other arrangement to an

Molecular Dynamics of a Polymer in Mixed Solvent

J. Phys. Chem. B, Vol. 109, No. 33, 2005 **15717**

Figure 3. The normalized $P_2(t)$ frequency between the consecutive side rings obtained from the simulation at 300, 330, and 360 K.

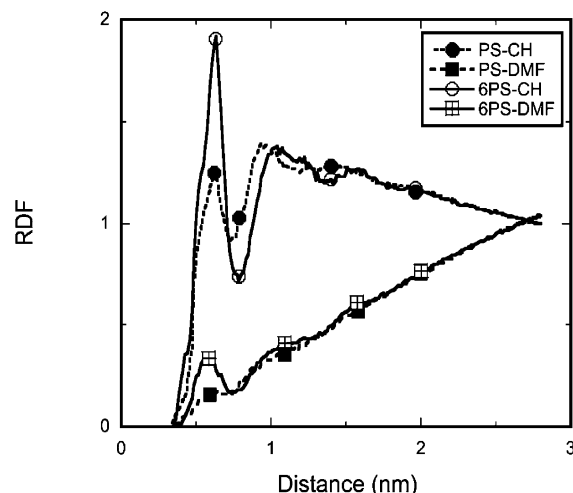**Figure 4.** Centers of monomers in tail–head conformation.

Figure 5. RDF of center of mass of PS backbone carbon and side ring carbon to CH and DMF at 300 K.

almost parallel one. Since the nonbonded Lennard-Jones interaction leads to the rings avoiding each other, the phenyl rings have to take parallel positions when located at the same side of the chains and the distance is small. They can be perpendicular satisfying the quadrupolar interaction at larger distances. It is interesting that the two peaks are very pronounced so that intermediate positions are negligible. Since parts of the solvents have an electrostatic interaction with the phenyl rings, the angles of the side ring plane are more likely to be parallel to accommodate the solvent molecules, as confirmed later when the *N*,*N*-dimethylformamide moves closer to phenyl rings as temperature increases.

Radial distribution functions, which measure the number of atoms (or molecules) in the vicinity of another atom (or molecule) at a given distance, were employed to reveal the local structures of PS in solution. To characterize the local structure around PS monomers, a monomer is represented either by the second backbone carbon or the center of the side ring at the monomer, therefore each PS chain will be represented as a "molecule of 15 atoms". Figure 4 shows how the centers are defined. We calculate the radial distribution functions between such centers. The centers of CH and DMF are the geometric centers of all 18 or 12 atoms, respectively; note that this is slightly different from the center of mass. The RDF of the second backbone carbon is represented as "PS" and RDF of the side groups is defined as "6PS" throughout the following analysis.

The first question we would like to answer is which part of PS is best solvated. Both molecules are more likely to target

the phenyl ring rather than the backbone at all temperatures and concentrations. One PS chain solvated in a CH and DMF solvent mixture at 300 K is taken as an example to show this trend in Figure 5. Figure 5 shows that PS and DMF or CH can approach as close as 0.2 nm. At distances of more than 2.7 nm the RDF approaches 1, indicating system homogeneity. There is a slope at the distance of 2.7 nm because of a finite size effect. We also performed simulations on 8-fold increased system sizes for select state points (see below) and confirmed that this finite size effect is weak. Both radial distribution functions with cyclohexane, PS–CH and 6PS–CH, have clearly stronger peaks than PS–DMF and 6PS–DMF. At a given distance, there is more CH than DMF surrounding the PS, the exact location of the PS center does not matter. This is consistent with CH being a good solvent for PS. By comparing PS–CH to 6PS–CH and PS–DMF to 6PS–DMF, we determine which part of the PS is the primary target. The RDF for the side ring to CH can get as high as 1.8 whereas that to the backbone carbon center is only 1.2. The integral under the curve from a distance of 0.5 to 0.8 nm of 6PS–CH is about 2.5 times that of PS–CH, which means that the total number of CHs around the side ring centers is about 2.5 times as that of CHs around the backbone carbons. The same trend shows that the $g(r)$ of the side ring center to DMF is 0.6 compared to 0.3 for backbone carbon. The integral under the first peak of 6PS–DMF is about twice bigger than that of PS–DMF. Both sets of data clearly show us that solvents favor the side ring over the backbone of PS.

We now address the temperature dependence of solvent quality. It is shown in Figure 6 that PS dissolves much more readily in CH than in DMF at lower temperatures (300 K), while at the higher temperature (330, 360 K) the solvation preference is not as strong. The ratio of the first peak in $g(r)$ between 6PS to CH and DMF at 300 K is approximately as big as 7.6, and it decreases to 2.3 and 1.6 respectively at 330 and 360 K. At room temperature, CH gathers around PS more and when the temperature increases, DMF gets closer. With increasing temperature small solvent molecules more readily overcome barriers leading to a locally more homogeneous system. At the same time, the polymer molecules tend to have changes in the local side ring conformation or the global chain scale to accommodate the solvents.

Next, the concentration dependence is evaluated for 1, 3, and 10 PS chains dissolved in the same number of small molecules at 300, 330, and 360 K. The system with only one chain is a
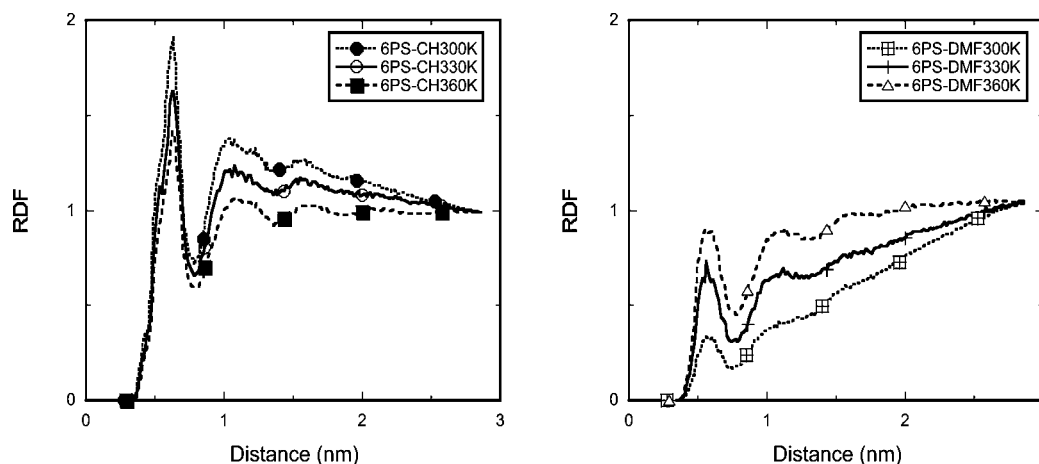
Figure 6. RDF of the center of mass of the side ring carbon to CH (left) and DMF (right) at 300, 330, and 360 K.
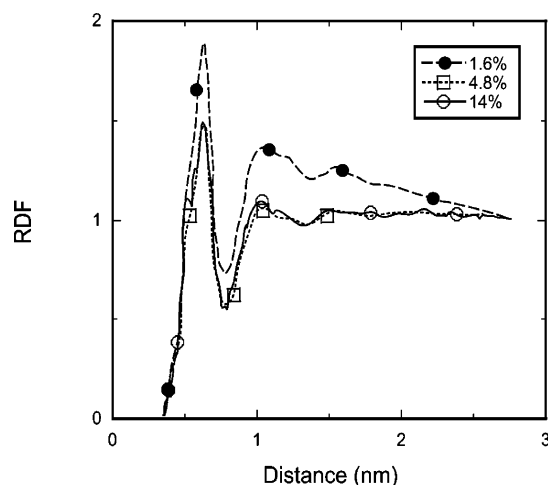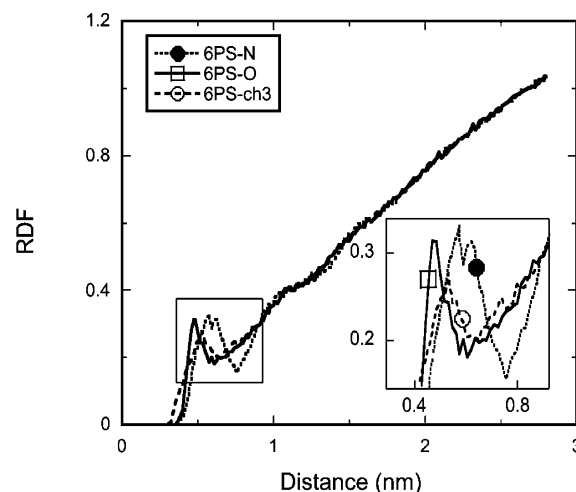

Figure 7. The RDF of the center of mass of PS side ring carbons to CH at 300 K at concentrations of 1.6%, 4.8%, and 14% (by weight).

Figure 8. RDF of the center of mass of PS side ring carbons to the N, O, and methyl group of DMF at 300 K and a concentration of 1.6%.

dilute solution, while for higher concentrations this is not immediately clear. The RDF of the center of mass of the side ring to CH at 300 K at concentrations of 1.6%, 4.8%, and 14% are plotted in Figure 7. In all three concentrations, the first peak occurs at around 0.6 nm, which represents the first solvation shell. Even though the peak from each concentration occurs at the same distance, the heights are different. While 1.6% corresponds to a peak height of RDF ≈ 1.85, the 4.8% and 14% concentrations have lower peaks height of RDF ≈ 1.5. The differences in height may be a result of the properties of the dilute polymer solution with one chain. In this case, all of the CH molecules are likely to remain close to the few side rings. As the polymer concentration increases, the ratio between the number of CHs and the side groups decreases, and there is now competition between chains for the better solvent. There is little difference between the RDFs of the 4.8% and 14% concentrations and we can take this as an indication that a moderate increase in PS does not dramatically change the system. Generally as concentration is increased, polymer coils come closer together and start to overlap. The concentration $\rho*$ at which the overlap starts is estimated as:[30]

$$\frac{\rho* N_A}{M} \frac{4}{3} \pi \cdot R_g^{\ 3} \cong 1$$

In our case the gyration radius of PS is around 0.8−1.0 nm. Thus, for a 15-monomer oligomer with a molecular weight M = 1562 g/mol, $\rho*$ can be as small as 5−20% in weight. The

weight concentration of one 15-monomer PS in a solvent mixture of 674 CH (with molecular weight = 84 g/mol) and 500 DMF (with molecular weight = 73 g/mol) molecules is 1.6%. With a concentration clearly lower than $\rho*$, this system can safely be classified as a dilute polymer solution. The weight concentration of three chains in the same mixture is 4.8% and may be at the boundary between a dilute and a semidilute solution. The upper concentration limit for this regime limit is the melt case without any solvent molecules. All our systems are clearly well away from this limit.

To determine how DMF approaches polystyrene, the RDF of the side rings with the nitrogen, the oxygen, and the methyl groups are calculated. A concentration of one chain at 300 K is taken as an example to elucidate the microscopic characteristics and the data are shown in Figure 8. O is found to be closest to the side rings, N is the farthest from the side rings, and methyl groups are intermediate. This can be explained by DMF being located between two consecutive phenyl rings. The O is then positioned nearest to the phenyl rings due to the electrostatic attraction between the charged O and the quadruples of the phenyl groups, while the methyl group is at the other end of the DMF, and will inevitably come close to another side ring. Thus, the methyl peak will be very similar to oxygens and the difference in peak distance between N and either O or the methyl group may be explained by the geometrical bond distance. The ratio of areas underneath the first RDF peak of 6PS−N, 6PS−O, and 6PS−ch3 is 1:1:2 consistent with the chemical formula.
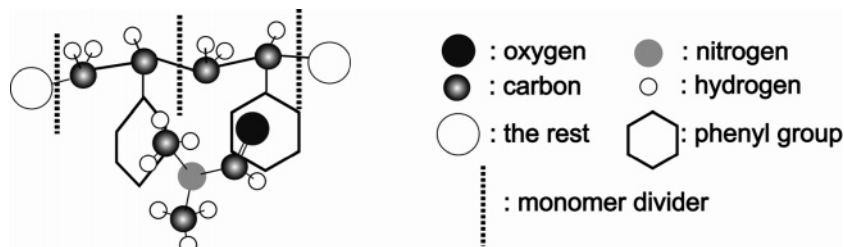
Molecular Dynamics of a Polymer in Mixed Solvent

J. Phys. Chem. B, Vol. 109, No. 33, 2005 **15719**

Figure 9. Sketch of how DMF is located near the PS chain.
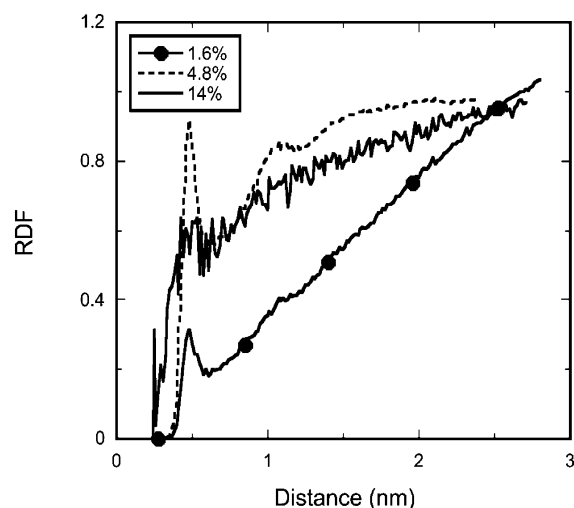

Figure 10. RDF of the center of mass of the PS side ring carbons to O of DMF at 300 K at concentrations of 1.6%, 4.8% and 14% (by weight).

The double peak structure in the first peak of 6PS−ch3 represents that two methyl groups are involved. Figure 9 shows a sketch of how DMF may be located near a PS chain consistent with our analysis.

The concentration dependence of the DMF−PS interaction process is investigated by examining the RDF of the phenyl rings with the oxygen atom at 300 K; all concentrations are shown in Figure 10. It is shown that the maximum of $g(r)$ increases from 0.3 to 0.9 as the concentration increases from 1.6% to 14% (by weight). Even though DMF is not a good solvent for PS, an increase in polymer concentration in the solution forces the O atoms and the centers of PS side rings closer to each other. Despite the noise, it is clear that as the concentration approaches our highest value, the peak is less noticeable and the remaining tail flattens. A concentration increase makes the solution more homogeneous bringing the DMF closer to the polymer. To check for finite size effects, solutions at 330 K are taken as an example and compared against an eight times bigger system at a 1.6% concentration. It is shown in Figure 11 that after 3 nm, the RDF of this system approaches 1, which means that the system achieves homogeneity. All the other characteristics are consistent with the smaller system showing that finite size effects are minor.

The global structure of PS cannot be fully described without the end-to-end distance. The end-to-end distance distribution at 1.6% was measured and is plotted in Figure 12 for our temperatures. When the temperature increases, the end-to-end distribution becomes broader indicating the chain becoming more flexible. The end-to-end distance reaches values as small as 0.3 nm at 360 K compared with 1.2 and 1.0 nm at 300 and 330 K. The end-to-end distance is capable of stretching out as long as 3.2 nm and at the same time the two ends of polymers are prone to coming closer as the polymer chain becomes more
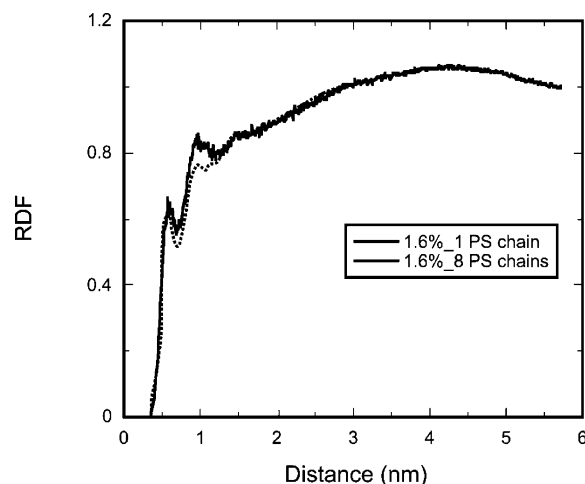

Figure 11. RDF of the center of mass of PS backbone carbon to nitrogen of DMF at a concentration of 1.6% at 330 K.
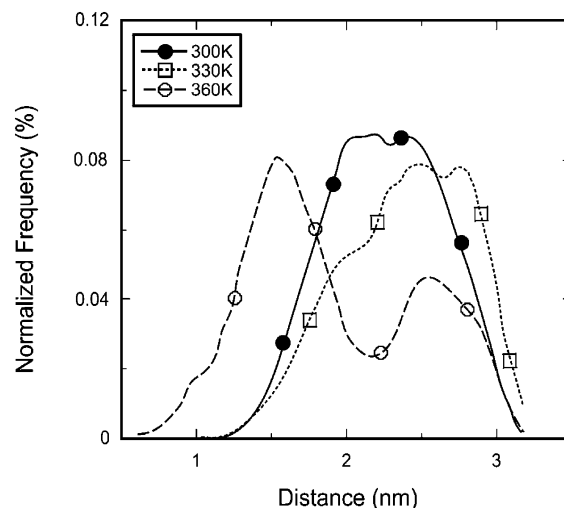

Figure 12. The end-to-end distance of the carbon of PS at a concentration of 1.6% at different temperatures.

flexible. The segments interact with their neighbors along the chain, distant segments interact if they come close to each other, and the polymer swells as long as the repulsive forces between segments dominate. This effect was introduced by Flory[31,32] and leads to the well-known $\langle R^2 \rangle \propto N^{1.2}$ law for the end−end distance of polymers in good solvent. The conformations of polymers can be experimentally studied by, e.g., light scatter-ing.[33] The single chain structure is defined as

$$S(q) = \frac{1}{N}\sum_{m=1}^{N_C}\langle|\sum_{j=1}^{n_b}\exp(iqr_j^m)|^2\rangle$$

where N_C is the number of chains, m is the chain index, N is the total number of monomers, $n_b = N/N_C$ is the number of
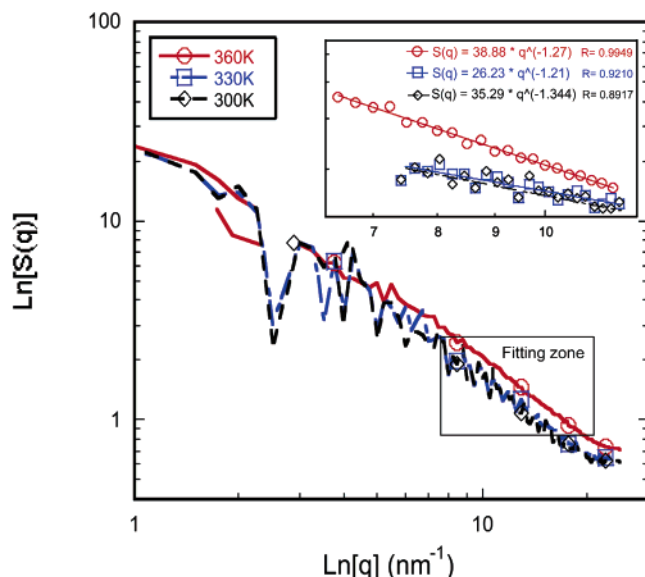
Figure 13. The structure factor of single chains of PS at different temperatures.

monomers along the chain, and j is the monomer index along the chain. Normally $S(q)$ decays with $q^{-1/\nu}$, where $d = 1/\nu$ is the fractal dimension of the chain. The fractal dimension depends on the structure of the chains which could, e.g., take a random coil structure or assume a rodlike structure. The concentration of the system influences the fractal dimension as well. We measured the structure factor at different temperatures. The fractal dimensions of one PS chain took on values of 1.27, 1.21, and 1.33 corresponding to 360, 330, and 300 K as shown in Figure 13. A chain with a value of $\nu = 1$ means the polymer is fully stretched while a chain with a value of $\nu = 2$ describes a random walk. All our fractal dimensions were between these two limits and closer to a stretched conformation, which is not surprising for our short oligomers. This provides a quantitative microscopic description for our observation since stretched conformations were more frequently observed by visual inspection. The fractal dimension does not show strong temperature dependence.
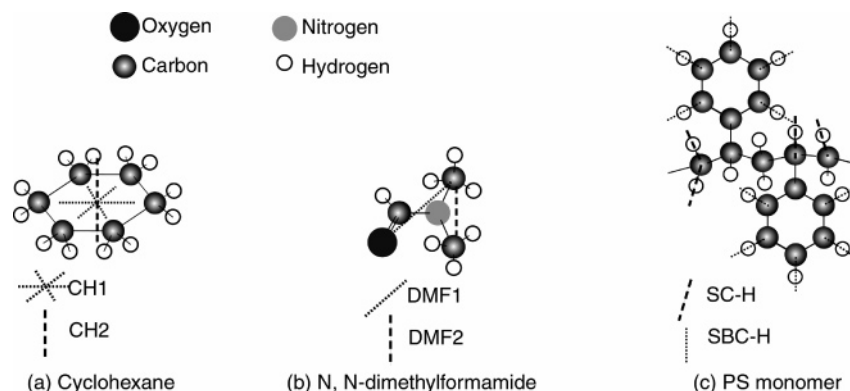
5. Dynamics of the System

Various experimental methods have been employed to characterize molecular reorientations. Infrared spectroscopy (IR), Raman, Rayleigh, and NMR spectroscopy[33] are important methods in molecular physics for the investigation of molecular movements and intermolecular correlations in liquid solutions. Dynamic as well as static properties are affected by changes in

both temperature and concentration. Orientation correlation functions, which elucidate the speed of reorientation, were used to evaluate the local dynamics from a molecular perspective. The second Legendre polynomial $P_2(t)$ expresses the decorrelation of the bond vector u and is defined as:

$$P_2(t) = C_{OCF} = \frac{1}{2}(3[\vec{u}(t)\cdot\vec{u}(0)]^2 - 1)$$

$\vec{u}(0)$ and $\vec{u}(t)$ are unit vectors at time 0 and t, respectively. Since the motion of the bond vector is not isotropic, a simple exponential does not fit the correlation process. The correlation functions can often be represented by a stretched exponential fit[15] or a sum of a single and a stretched exponential fit,[34] and the correlation times are defined as the time integral over the correlation functions. In this section the vectors are defined as in Figure 14: We use eight vectors to describe the dynamics in the system: **CH1** is the vector that connects two opposite carbons in the cyclohexane plane. There is no difference among the three in-plane vectors due to symmetry. **CH2** is the vector perpendicular to the cyclohexane plane and indicates how the cyclohexane plane flips. It is defined as the cross product of any two in-plane **CH1** vectors. In DMF, **DMF1** is the vector that connects the aldehydic oxygen and one of the methyl group carbons, and **DMF2** is the vector that connects the two carbons of the methyl group. **bk** is the vector that connects consecutive backbone carbons in the polymer, **end−end** is the vector connecting the two terminal carbons of PS; **SC−H** is the vector that connects the backbone carbons with directly bonded hydrogens; and **SBC−H** is the vector that connects the phenyl carbons with the hydrogens on the side ring.

The objective is to understand the dynamic properties of the polymer mixture system in detail. The eight vectors are investigated to characterize the motion of CH, DMF, and PS and to evaluate the temperature and concentration dependences. Paralleling the 1.6% at 330 K, a second PS system with a different atactic arrangement is studied to have better statistics. To avoid end effects, the two monomers at either end are excluded from the calculation of the segmental vectors, so statistically 11-monomer PS chains are averaged. The resulting correlation times and statistic errors are listed in Table 4. The errors are calculated as the following: For the multichain polymeric systems, the correlation times of each individual chain are calculated and the maximum absolute difference of the same vector among the chains is considered and listed as errors. For the single chain system at 300 and 360 K, the errors come from the difference of times measured in the first and second half of the run. For the single chain system at 330 K, the relaxation times are compared with those of the paralleling system. All

Figure 14. definition of investigated vectors.

Molecular Dynamics of a Polymer in Mixed Solvent

J. Phys. Chem. B, Vol. 109, No. 33, 2005 **15721**

TABLE 4: Correlation Times (ps) of Different Vectors

τ_{cor}		CH1	CH2	DMF1	DMF2	end	bk	SC−H	SBC−H
300 K	1mix	2.72 ± 0.09	4.46 ± 0.15	3.43 ± 0.17	2.95 ± 0.15	826 ± 85	309 ± 81	229 ± 56	210 ± 38
	3mix	2.71 ± 0.17	4.65 ± 0.08	3.45 ± 0.16	3.11 ± 0.07	740 ± 64	503 ± 82	437 ± 62	389 ± 45
	10mix	3.00 ± 0.08	6.23 ± 0.03	4.02 ± 0.16	3.33 ± 0.04	1137 ± 24	716 ± 13	595 ± 25	520 ± 15
330 K	1mix	2.55 ± 0.09	3.28 ± 0.02	2.74 ± 0.08	2.78 ± 0.06	852 ± 72	$264/564^a$	$207/482^a$	$164/365^a$
	3mix	1.90 ± 0.03	2.91 ± 0.05	2.33 ± 0.21	2.22 ± 0.13	491 ± 24	274 ± 35	221 ± 33	192 ± 27
	5mix	2.66 ± 0.06	3.58 ± 0.01	2.84 ± 0.15	2.93 ± 0.23	710 ± 96	407 ± 20	354 ± 59	301 ± 50
	10mix	2.05 ± 0.02	3.58 ± 0.04	2.71 ± 0.06	2.38 ± 0.02	791 ± 57	379 ± 12	307 ± 19	266 ± 11
360 K	1mix	2.24 ± 0.06	2.63 ± 0.15	2.39 ± 0.06	2.36 ± 0.09	465 ± 31	155 ± 16	99.7 ± 17.8	102 ± 6
	3mix	1.53 ± 0.07	2.10 ± 0.11	1.84 ± 0.03	1.68 ± 0.06	290 ± 12	179 ± 42	142 ± 46	119 ± 26
	7mix	2.28 ± 0.04	2.97 ± 0.01	2.57 ± 0.11	2.42 ± 0.06	318 ± 49	193 ± 25	173 ± 19	145 ± 21
	10mix	2.37 ± 0.11	2.96 ± 0.12	2.45 ± 0.03	2.43 ± 0.10	362 ± 20	196 ± 33	151 ± 18	137 ± 14

^{a} These values are correlation times from chains with different local structures, no error is applied here.

the correlation times are consistent within tolerance except the local **bk**, **SC−H**, and **SBC−H** vectors. This results show that the explicit architecture can have a marked influence on the local dynamics, but the global dynamics of the end-to-end vector is almost unaffected even for oligomers. Segments in racemic dyads are generally faster than meso. For example, the correlation time of "bk" vectors in a 1mix system with nine racemic dyads averages to 267 ps compared to 564 ps with five. Only the average correlation times of bk, SC−H, and SBC−H at 330 K are listed in Table 4. We find that the correlation times of CH and DMF increase with polymer content and decrease with temperature. For CH2 vectors at 300 K, the correlation time increases from 4.46 to 4.65 ps and 6.22 ps as the concentration increases; for CH1 vectors at the lowest concentration, the correlation time decreases from 2.72 to 2.55 ps to 2.24 ps as the temperature increases. Since the polymers are expected to act as obstacles to the solvent molecules, their presence slows down the motion of small molecules[7] and thus the correlation times increase. Another noticeable feature is the dramatic difference between the four solvent vectors. For the two vectors of CH, the dynamics of the in-plane vector changes much less than the normal vector with temperature and polymer concentration. The CH1 correlation time decreases by a factor of 1.1 from 300 to 330 K, whereas for CH2 the speedup is 1.3. This is a result of the molecular geometry, where a symmetry in-plane structure requires much less rotational activation energy and room for movement than the reorientation of the normal vector. The correlation time for a normal vector changes more dramatically than the in-plane vector of CH. We also used two vectors to represent the motion of DMF. These two vectors are approximately perpendicular to each other in space. The vector corresponding to a longer distance, DMF1, is slower than DMF2.

A similar temperature tendency was seen for the four vectors (end−end, backbone, SC−H, and SBC−H) along the polymers. The end−end vector, which is the longest global vector, was expected to be the slowest. The backbone vector, which is a segmental vector that defines the characterizing movement of the backbone carbon, is expected to decay faster. Both the SC−H and SBC−H vectors are expected to be even faster as the segmental motion and local librations superimpose. The correlation times for all four vectors decrease with temperature at constant concentration as expected. However, the vectors show different concentration behaviors. We take a representative example of a 1PS chain here at 300 K with correlation times of 826, 309, 229, and 210 ps for end−end, backbone, SC−H, and SBC−H, respectively. The four different vectors show different concentration dependencies. For the end−end vector at 300 K, the correlation time decreases from 826 ps to 740 ps as the concentration changes but increases to 1137 ps when the concentration increases to 10mix. The correlation time increases

with concentration since the chains hinder each other more strongly, which as a result slows down the dynamics. This result was seen in the correlation times that corresponded to the 3mix and 10mix concentrations. As for the correlation time decrease that occurred when the concentration was increased from 1mix to 3mix, this may have been the result of different dynamics. As reported by Hanson et al., the dynamics of polystyrene in formamide solvent involves bimodal relaxation of the correlation function in the dilute to semidilute regime.[35] To describe the dynamics of polymers in dilute solution, we have to take into account the hydrodynamic interaction, as by the Zimm model.[30] This model predicts the molecular weight dependence of the rotational relaxation time τ_r as

$$\tau_r \propto M^{3/2}.$$

In dilute solution, the polymer−polymer interaction has only a small effect. The 1.4% concentration has only one polymer inside the solution and there is virtually no polymer−polymer interaction at all. However, there still are strongly correlated fluctuations between polymer segments. A semidilute solution is characterized by large and strongly correlated fluctuations. One can calculate the relaxation time τ_r in semidilute solution as

$$\tau_r = \tau_1^{(0)} p^{-3/2}\left(1 + Ac\left(\frac{p}{N}\right)^{-\mu} + ...\right)$$

where $\tau_1^{(0)}$ is the longest relaxation time in the dilute limit ($c \rightarrow 0$) and $\mu \cong 0.5$. This equation explicitly shows that the p dependence of τ_p changes from $\tau_p \propto p^{-3/2}$ to $\tau_p \propto p^{-2}$ as the concentration increases.[30] Due to the change in power, there is a point where increasing the concentration actually decreases the correlation time, which we see going from 3 to 10 chains. A polymer melt would be the high concentration limit in which the polymer coils come fully together and can be treated by mean field theory. For the backbone vectors connecting the two consecutive backbone carbons, the correlation time does not show a consistent trend. At 300 K, the correlation times of the backbone vectors increase from 309 ps to 716 ps and from 155 ps to 196 ps at 360 K when the concentration increases from 1 to 10 chains. As segmental vectors represent much shorter movements compared with the global end−end vectors, the backbone vectors do not show the same dynamic mechanism as the global dynamics. At the same time, their length scale of bk vectors is very close to that of local vectors, and thus effects overlap. The other two local vectors, SC−H and SBC−H, represent the motion of the backbone carbon to hydrogen and side ring carbon to side ring hydrogen. These C−H vectors oscillate about their energy minimum without crossing any conformational barriers. This vibration is affected predominantly

TABLE 5: Activation Energy

E_a (kJ/mol)	CH1	CH2	DMF1	DMF2	end	bk	SC−H	SBC−H
1mix	2.82	8.01	5.52	3.15	6.54	8.74	9.59	9.71
3mix	8.82	12.18	9.74	9.22	13.07	15.90	17.57	18.40
10mix	4.35	12.30	8.11	5.37	14.32	18.51	19.41	19.23

TABLE 6: Rate Factor

A^a	CH1	CH2	DMF1	DMF2	end	bk	SC−H	SBC−H
1mix	8.89	1.79	3.72	8.47	638.63	95.7	51.36	43.54
3mix	0.78	0.35	0.69	0.77	39.40	8.50	3.78	2.41
10mix	4.98	0.44	1.52	3.75	37.20	4.27	2.48	2.32

a 1e−13 cm²/s.

by either the solvents or the polymer segments that surround these vectors. Thus our simulation data do show a satisfactory description of this trend. Overall all the segmental vector and local vectors show a similar temperature and concentration dependence, that is, the correlation times of both vectors increase with concentration and decrease with rising temperature.

To understand the temperature dependence of the correlation times, we also used an Arrhenius description.
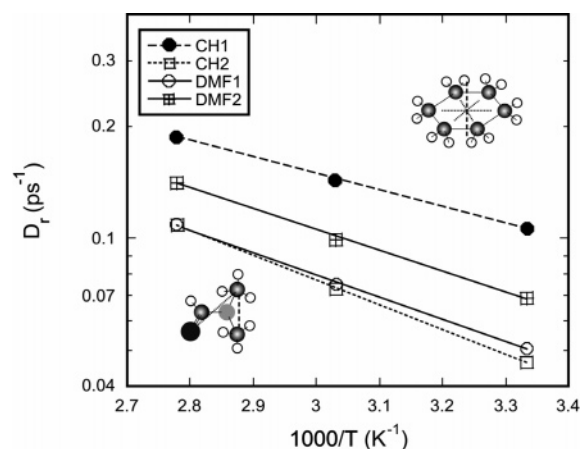
$$k = A \exp(-E_a/RT)$$

E_a is the activation energy and A the rate factor. The correlation times for the three temperatures can be used in connection with the Arrhenius law to find the activation energy. The activation energy of the correlation time and rate factors are calculated from the exponential fits and listed in Tables 5 and 6 separately. We take an example of the lowest concentration to elucidate the motion of defined vectors. The activation energies of CH1, CH2, DMF1, and DMF2 in 1mix PS solution are 2.82, 8.01, 5.52, and 3.15 kJ/mol, respectively. The in-plane rotation needs to overcome a lower barrier compared to the flipping. The two vectors representing the motion of DMF have very similar energy barriers. There is a 60−80% increase in activation energy as the concentration increases from 1 to 3 chains for all four vectors. This stems from the fact that the presence of the ten PS chains greatly limits the motion of the small molecules, compared to the lower concentrations. The activation energies of both SC−H and SBC−H are the highest at all concentrations. One can notice that the activation energies and rate factors do not always show a consistent trend in the reorientation, indicating that both parameters determine the movement of given vectors independently. For example, associated with highest activation energies of both SC−H and SBC−H vectors, the rate factors of those vectors have values much lower than those of end−end or bk. The overall reorientation of SC−H and SBC−H is much faster than that of the end-to-end or backbone carbons after both parameters are taken into account.

The discussion of solvent dynamics would not be complete without characterizing the motion of the molecules as a whole. The diffusion coefficients, which tell us how fast the particle moves, were calculated for CH and DMF and are listed at Table 7. Figures 15 and 16 illustrate how the correlation times change

Figure 15. Logarithm plot of the rotational diffusion constants of solvents to $1/T$ at a concentration of 1.4%.
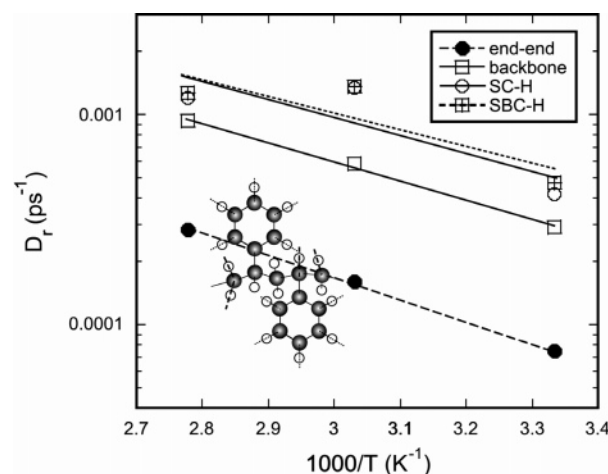
Figure 16. Logarithm plot of the rotational diffusion constants of PS chains to $1000/T$ at concentration of 1mix.

with temperature. The self-diffusion constant of the center of mass is expressed as

$$D = \lim_{t \to \infty} \frac{1}{6t} \langle (R(t) - R(0))^2 \rangle$$

where $R(t)$ is the position at time t. The diffusion coefficient for CH at 300 K in this model was found to be 0.998×10^{-5} cm²/s. The value of 0.89×10^{-5} cm²/s reported by Schmitz[36] is about 10% lower; the value of 0.76×10^{-5} cm²/s was found at the condition of 500 CH in the neighborhood of one trans-polyisoprene.[7] This is because the mobility of the CH depends strongly on the size and concentration of the molecules with which it is mixed. After comparing the diffusion constants of any two carbons that are directly opposite each other in plane, we found that the diffusion of CH was completely isotropic. At the same time, the diffusion of DMF was anisotropic at small times taking the N, O atoms of DMF as examples. The diffusion distances of CH with one chain in 0.6 ns were 4.0 nm at 300 K

TABLE 7: Diffusion Constant of Solvent Mixture

D^a	300 K		330 K		360 K	
	CH	DMF	CH	DMF	CH	DMF
1mix	0.998 ± 0.028	1.038 ± 0.052	1.762 ± 0.184	1.810 ± 0.069	2.699 ± 0.375	3.121 ± 0.414
3mix	0.885 ± 0.059	1.009 ± 0.226	1.550 ± 0.015	1.702 ± 0.018	2.394 ± 0.203	2.613 ± 0.102
10mix	0.654 ± 0.003	0.812 ± 0.093	1.265 ± 0.011	1.595 ± 0.008	1.961 ± 0.048	2.426 ± 0.152

a 1e−5 cm²/s

Molecular Dynamics of a Polymer in Mixed Solvent

J. Phys. Chem. B, Vol. 109, No. 33, 2005 **15723**

TABLE 8: Activation Energy of Diffusion

$E_{act.}$ (kJ/mol)	CH	DMF
1mix	14.63	16.95
3mix	14.71	14.19
10mix	15.77	15.54

with an average box length of 5.67 nm, 6.66 nm at 330 K with a box size of 5.74 nm, and 10.23 nm at 360 K with a box size of 5.83 nm. It showed clearly that CH diffused much faster at elevated temperatures. The same temperature dependence was found in the diffusion constant for DMF. Overall, the diffusion of both small solvents showed a much stronger dependence on temperature than the reorientation. More space is needed for diffusion than rotation, which can sometimes take place in place as well. Both CH and DMF have similar concentration dependences. The diffusion movements slowed strongly when more PS chains were around as PS chains acted as obstacles to the solvents and made their dynamics more difficult. The activation energies of diffusion were also calculated and are shown in Table 8. These activation energies are on the order of $E_{act} = 10$ kJ/mol. The diffusion activation energies of CH increase with concentration. An increase in polymer chain concentration makes the CH diffusion much harder during the process of CH migration toward the PS side rings. DMF does not form favorable interactions with the PS chains. At the lowest concentration, DMF is far away from the PS chain as seen in the RDF and it had the largest diffusion energy. DMF molecules were initially located away from the polymer and it was very hard for them to move to the polymer side. As the concentration increased to 3 chains, the PS solution was in the semidilute case and DMF molecules were located closer to PS chains thus increasing the repulsive forces between PS and DMF. These interactions caused the DMF molecules to be unfavorable near the PS chains and they could easily drift away. As the PS concentration increased further to 10, movement from one spot to another became harder since the increase in PS chain monomers posed a formidable barrier for the DMF to overcome. Thus the microscopic interactions and conformations are the leading factors in diffusion movement.

6. Conclusion

We have investigated the local structure and dynamics of PS in a mixed solvent. We presented the distance and angle distributions. We found that the two consecutive side rings are in a perpendicular position and are prone to parallel each other due to the quadrupolar interaction.

The solvation is analyzed in detail: PS side rings are the primary targets for the solvents. PS chains have a strong preference to CH over DMF. When temperatures increase, DMF molecules get closer. Oxygen of the DMF is found to be the nearest to the centers of PS side rings with methyl groups of DMF consequently close to other side rings. As concentration increases, different mechanisms are involved in the solvation process and the lowest concentration is considered a dilute solution and the higher ones can be considered semidilute. The structure of the PS chain is closer to a stretched conformation than a random walk.

The dynamics of the polymeric solution are studied by correlation times and activation energies associated with the reorientation. Increasing temperatures speeds up the movement of all the small molecules and increasing concentrations slows down the reorientation process. Different vectors from PS show

different temperature and concentration dependences: segmental and local movements of PS show the same temperature and concentration dependences as solvents vectors, while the correlation time of the end-to-end vector decreases as concentration increases. This is because different mechanisms are involved during the change from a dilute to a semidilute solution. The diffusion constants and activation energies of diffusion of small solvents are analyzed and it shows that the microscopic interaction dominates the movement of the small molecules and their reaction to concentration.

References and Notes

(1) Ward, I. M., Ed. *Structure and Properties of Oriented Polymers*; Applied Science: London, UK, 1978.

(2) Sun, H. *J. Phys. Chem. B* **1998**, *102*, 7338.

(3) Mooney, D. A.; Müller-Plathe, F.; Kremer, K. *Chem. Phys. Lett.* **1998**, *294*, 135.

(4) McDonald, N. A.; Jorgensen, W. L. *J. Phys. Chem. B* **1998**, *102*, 8049.

(5) Perico, A.; Moe, N. E.; Ediger M. D. *J. Chem. Phys.* **1998**, *108*, 1245.

(6) Müller-Plathe, F. *Chem. Phys. Lett.* **1996**, *252*, 419.

(7) Faller, R. *Phys. Chem. Chem. Phys.* **2002**, *4*, 2269.

(8) Fukao, K.; Mayamoto, Y. *Polymer* **1993**, *34*, 238.

(9) Mansour, A. A.; Happ, E.; Wolf, T.; Stoll, B. *Colloid Polym. Sci.* **1994**, *272*, 894.

(10) Kuebler, S. C.; Heuer, A.; Spiess, H. W. *Phys. Rev. E* **1997**, *56*, 741.

(11) He, Y.; Lutz, T. R.; Ediger, N. D.; Ayyagari, C.; Bedrov, D.; Smith, G. D. *Macromolecules* **2004**, *37*, 5032.

(12) Mondello, M.; Yang, H. J.; Furuya, H.; Roe, R. J. *Macromolecules* **1994**, *27*, 3566.

(13) Roe, R. J. *J. Non-Cryst. Solids* **1998**, *235−237*, 308.

(14) Han, J.; Boyd, R. H. *Polymer* **1996**, *37*, 1797.

(15) Ayyagari, C.; Bedrov, D.; Smith, G. D. *Macromolecules* **2000**, *33*, 6194.

(16) Lyulin, A. V.; Balabaev, N. K.; Michels, M. A. J. *Macromolecules* **2002**, *35*, 9595.

(17) Liu, Z.; Pan, C.; Lodge, T. P. *Macromolecules* **1995**, *28*, 3221.

(18) Auroy, P.; Auvray, L. *Langmuir* **1994**, *10*, 225.

(19) Sackin, R.; Ciampi, E.; Godward, J.; Keddie, J. L.; McDonald, J. P. *Macromolecules* **2001**, *34*, 890.

(20) Tsunashima, Y.; Hirata, M.; Nemoto, N.; Kurata, M. *Macromolecules* **1988**, *21*, 1107.

(21) Einaga, Y. *Prog. Polym. Sci.* **1994**, *19*, 1.

(22) Gao, J.; Pavelites, J. J.; Habibollazadeh, D. *J. Phys. Chem.* **1996**, *100*, 2689.

(23) Lindahl, E.; Hess, B.; Spoel, D. V. D. *J. Mol. Model.* **2001**, *7*, 306.

(24) Chalaris, M.; Samios, J. *J. Chem. Phys.* **2000**, *112*, 8581.

(25) Jorgensen, W. L.; Severance, D. L. *J. Am. Chem. Soc.* **1990**, *112*, 4768.

(26) Hess, B.; Bekker, H.; Berendsen, H. J. C.; Fraaije, J. G. E. M. *J. Comput. Phys.* **1997**, *18*, 1463.

(27) Faller, R.; Schmitz, H.; Biermann, O.; Müller-Plathe, F. *J. Comput Chem.* **1999**, *20*, 1009.

(28) Park, H. *Polymer* **1999**, *40*, 2003.

(29) Berendsen, H. J. C.; Postma, J. P. M.; Gunsteren, V.; DiNola W. F. A.; Haak, J. R. *J. Chem. Phys.* **1984**, *81*, 3684.

(30) Doi, M.; Edwards, S. F. *The Theory of Polymer Dynamics*; Clarendon Press: Oxford, UK, 1986.

(31) Flory, P. J. *J. Chem. Phys.* **1949**, *17*, 303.

(32) Flory, P. J. *Principles of Polymer Chemistry*; Cornell University Press: Ithaca, NY, 1953.

(33) Spells, S. J., Ed. *Characterization of Solid Polymers*: *New Techniques and Developments*; Chapman & Hall: New York, 1994.

(34) Moe, N. E.; Ediger, M. D. *Phys. Rev. E* **1999**, *59*, 623.

(35) Hanson, E. T.; Borsali, R.; Pecora, R. *Macromolecules* **2001**, *34*, 2208.

(36) Schmitz, H.; Faller, R.; Müller-Plathe, F. *J Phys. Chem. B* **1999**, *103*, 9731.